Inorganic Chemistry

Article

pubs.acs.org/IC

Mechanistic Studies of Hydrogen Evolution in Aqueous Solution Catalyzed by a Tertpyridine–Amine Cobalt Complex

Anna Lewandowska-Andralojc,*[,†,§] Teera Baine,[‡] Xuan Zhao,[‡] James T. Muckerman,[†] Etsuko Fujita,[†] and Dmitry E. Polyansky*[,†]

[†]Chemistry Department, Brookhaven National Laboratory, Upton, New York 11973-5000, United States

[‡]Department of Chemistry, University of Memphis, Memphis, Tennessee 38152, United States

Supporting Information

ABSTRACT: The ability of cobalt-based transition metal complexes to catalyze electrochemical proton reduction to produce molecular hydrogen has resulted in a large number of mechanistic studies involving various cobalt complexes. While the basic mechanism of proton reduction promoted by cobalt species is well-understood, the reactivity of certain reaction intermediates, such as **Co^{I}** and **Co^{III}**–H, is still relatively unknown owing to their transient nature, especially in aqueous media. In this work we investigate the properties of intermediates produced during catalytic proton reduction in aqueous solutions promoted by the $[(DPA\text{-}Bpy)Co(OH_2)]^{n+}$ (DPA-Bpy = *N*,*N*-bis(2-pyridinylmethyl)-2,20-bipyridine-6-methanamine) complex ($[Co(L)(OH_2)]^{n+}$ where L is the pentadentate DPA-Bpy ligand or $[\mathbf{Co}(OH_2)]^{n+}$ as a shorthand). Experimental results based on transient pulse radiolysis and laser flash photolysis methods, together with electrochemical studies and supported by density functional theory (DFT) calculations indicate that, while the water ligand is strongly coordinated to the metal center in the oxidation state 3+, one-electron reduction of the complex to form a Co^{II} species results in weakening the Co–O bond. The further reduction to a Co^{I} species leads to the loss of the aqua ligand and the formation of $[\mathbf{Co^{I}}–VS)]^{+}$ (VS = vacant site). Interestingly, DFT calculations also predict the existence of a $[Co^{I}(\kappa^4\text{-}L)(OH_2)]^{+}$ species at least transiently, and its formation is consistent with the experimental Pourbaix diagram. Both electrochemical and kinetics results indicate that the Co^{I} species must undergo some structural change prior to accepting the proton, and this transformation represents the rate-determining step (RDS) in the overall formation of $[\mathbf{Co^{III}}–H]^{2+}$. We propose that this RDS may originate from the slow removal of a solvent ligand in the intermediate $[Co^{I}(\kappa^4\text{-}L)(OH_2)]^{+}$ in addition to the significant structural reorganization of the metal complex and surrounding solvent resulting in a high free energy of activation.

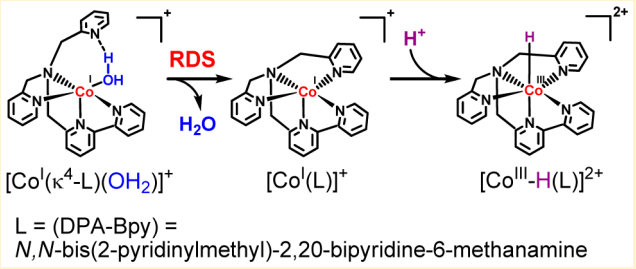

INTRODUCTION

The conversion of solar energy into fuels through photochemical water splitting is considered a viable solution to global energy problems and the reduction of anthropogenic emissions of carbon dioxide.[1,2] During the past decades, substantial effort has been made to develop catalysts for the reductive side of water splitting, that is, the generation of H_2 from protons and an electron source, using earth-abundant transition-metal complexes.[3−5] Molecular complexes based on cobalt (Chart 1),[6−22] nickel,[23−27] iron,[28−30] and molybdenum[31−34] have been shown to catalyze proton reduction in acidic acetonitrile (or, in a few cases, water) to produce H_2 under electro- and/or photochemical conditions in an efficient manner.

Cobaloxime complexes (**cat14**, **cat15**, **cat16**) have been extensively studied as catalysts for electrochemical[6−8] and photochemical[9−12] H_2 production owing to their relatively simple preparation and the low overpotentials required to reduce protons. Despite extensive mechanistic studies,[35,36] some details of cobaloxime-catalyzed proton reduction remain a topic of much debate, largely owing to the difficulty of detection of some key reactive intermediates such as the **Co^{III}**–H species. Several mechanisms for proton reduction promoted by cobaloxime complexes have been proposed in the literature.[5,36−39] Commonly two reductions, namely, Co$^{III/II}$ and Co$^{II/I}$, are followed by protonation of Co^{I} to yield a **Co^{III}**–H species.[3] In one proposed heterolytic pathway, protonation of the resulting **Co^{III}**–H yields H_2 and regenerates Co^{III} species. Fontecave and Artero originally suggested that this mechanism operates in the proton electroreduction with **cat14**.[7] They also reported that, depending on the applied potential and the pK_a of the acid used, different pathways for hydrogen production could operate.[40] In the proposed homolytic pathway, a bimolecular reaction involving two **Co^{III}**–H species results in H_2 release.[8,37,41] Eisenberg et al. proposed an alternative heterolytic pathway in which the **Co^{III}**–H is further reduced to a **Co^{II}**–H species that is subsequently protonated to generate H_2.[11,39] It is also believed that the mechanism can change, depending on the applied

Received: December 29, 2014
Published: April 22, 2015

DOI: 10.1021/ic5031137
Inorg. Chem. 2015, 54, 4310−4321

Chart 1. Selected Cobalt Complexes Reported As Catalysts for Proton Reduction

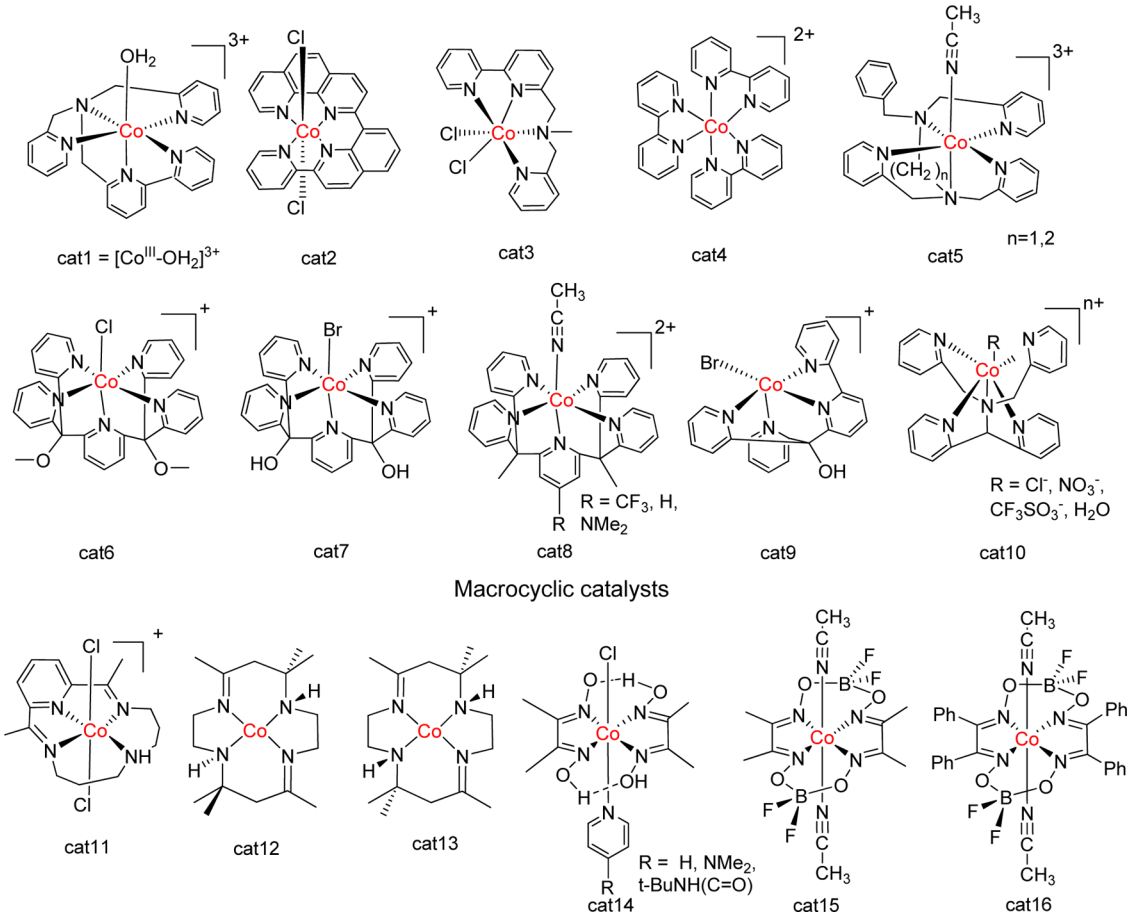

potential, concentration of the reducing agent, the concentration of the added acid, and the acid pK_a.

Several recent theoretical studies reported independently by the groups of Hammes−Schiffer[42,43] and Muckerman[44] have elucidated key mechanistic details for H_2 production by cobaloxime complexes. Both monometallic and bimetallic pathways were considered in these theoretical approaches, but the monometallic route in which **Co^{III}**−H is reduced to **Co^{II}**−H followed by protonation to generate H_2 and Co^{II} was determined to be the most plausible in terms of stabilities of presumed reaction intermediates.

A substantial body of literature describes cobaloxime systems in dry organic solvents with organic acids acting as a proton source. The use of organic solvents was usually justified by the poor solubility or instability of these cobalt complexes in water. A proton reduction catalyst that can perform effectively in pure aqueous media is highly desirable to couple proton reduction and water oxidation half reactions, and there are only a handful of molecular cobalt complexes known to efficiently catalyze water reduction in fully aqueous solutions.[15−20,45−53] Among those, Co complexes containing multipyridine ligand architectures have been reported in recent years, for example, including pentadentate: [(RPY5Me$_2$)Co(CH$_3$CN)]$^{2+}$ (RPY5Me$_2$ = 2,6-bis(1,1-bis(2-pyridyl)ethyl)pyridine, R = H, 4-CF$_3$, NMe$_2$) (**cat8**); [(DPA-Bpy)Co(Cl)]$^{2+}$ (DPA-Bpy = *N*,*N*-bis(2-pyridinylmethyl)-2,20-bipyridine-6-methanamine) (**cat1**); [(bztpen)-Co(CH$_3$CN)]$^{2+}$ (bztpen = *N*-benzyl-*N*,*N*′,*N*′-tris(2-pyridylmethyl)ethylenediamine) (**cat5**); [Co(N4Py)Cl]$^{2+}$ (N4Py = 1,1-di(pyridin-2-yl)-*N*,*N*-bis(pyridin-2-ylmethyl)-methanamine (**cat 10**); [Co(PPy-OMe)Cl]$^{+}$ (PPy-OMe = 6-(bis(bis-2-pyridyl)-methoxymethane) pyridine) (**cat6**); [Co-(PPy−OH)Cl]$^{+}$ (PPy−OH = pyridine-2,6-diylbis(dipyridin-2-ylmethanol) (**cat7**) and tetradentate: [Co(ppq)Cl$_2$] (8-(1″,10″-phenanthrol-2″-yl)-2-(pyrid-2′-yl)quinolone) (**cat2**); [Co(TPY−OH)(Br)]$^{+}$ (TPY−OH = 2-bis(2-pyridyl)-(hydroxy)methyl-6-pyridylpyridine) (**cat9**); and [Co(bpma)-(Cl$_2$)] (bpma = *N*-methyl-*N*-(2-pyridinylmethyl)-2,20-bipyridine-6-methanamine (**cat3**).[15−20,45−53]

Co-aqua complexes, e.g., **cat1** (see below) were found to be more stable in aqueous solutions, especially under acidic conditions, compared to the cobaloxime systems. In comparison to cobaloxime complexes, Co-polypyridyl catalysts have been mechanistically investigated to a lesser extent. A few studies of electrocatalytic or photocatalytic H_2 evolution with Co−polypyridyl based catalysts focused on the mechanistic and kinetic details, providing some understanding of the proton reduction steps.[13,22,46−48,52]

To provide further insight into the mechanism of proton reduction by **cat1**, Webster et al. performed density functional theory (DFT) calculations to explore possible reaction intermediates and the free-energy profiles of various proton reduction pathways.[15] The results from the DFT calculations suggested that a number of reaction pathways are thermodynamically feasible, leaving the question about the exact catalytic mechanism still open. In this work, we employed electrochemical, spectroscopic, transient laser flash photolysis, and transient pulse radiolysis studies to examine the mechanism of proton reduction by the **cat1** in aqueous media. The direct

DOI: 10.1021/ic5031137
Inorg. Chem. 2015, 54, 4310−4321

detection of key intermediates such as the Co^{I} species of **cat1** and the kinetics analysis of its transformation to the $[\mathbf{Co^{III}}-H]^{2+}$ intermediate provided a better understanding of the catalyst transformation steps in the overall catalytic reduction of protons to hydrogen.

EXPERIMENTAL SECTION

Materials. Tris(2,2′-bipyridine)ruthenium(II)chloride hexahydrate ($[Ru(bpy)_3]Cl_2{\cdot}6H_2O$) was obtained from Strem Chemicals, Inc. Ascorbic acid was supplied by Fisher. Sodium acetate, sodium perchlorate, monobasic and dibasic sodium phosphates, acetonitrile, and *tert*-butanol were supplied by Sigma-Aldrich. All chemicals used were 99% grade or higher and used without further purification.

Aqueous solutions were prepared with distilled water that had been passed through a Millipore ultrapurification system. Complexes $[Co^{II}(DPA\text{-}Bpy)Cl]Cl$ and $[Co^{III}(DPA\text{-}Bpy)(OH_2)](PF_6)_3$ were prepared using previously published methods.[15]

Density Functional Theory Calculations. All geometries were fully optimized at the B3LYP level of DFT[54−57] with the SMD aqueous continuum solvation model[58] using the all-electron 6-31G++(d,p) 5d basis set[59] on all atoms. Nonanalytical integrals were evaluated using the *integral = grid = ultrafine* option as implemented in the Gaussian 09 software package.[60] The nature of all stationary points was verified by analytic computation of vibrational frequencies, which were also used for the computation of zero-point vibrational energies, and thermal contributions to the free energies.

A 1 M standard state was used for all species in solution; thus, an adjustment for the 1 atm to 1 M standard-state concentration change of RT ln(24.5) (1.89 kcal/mol at 298 K) was added to the computed gas-phase free energies. In the case of water solvent, the 1 atm gas-phase free energy is adjusted by the sum of a 1 atm to 55.6 M standard-state concentration change, or 4.27 kcal/mol, and the experimental 1 M to 1 M self-solvation free energy, −6.32 kcal/mol, yielding an overall correction of −2.05 kcal/mol to the gas-phase free energy. The 1 M to 1 M solvation free energy of the proton was taken from experiment as −264.0 kcal/mol.[61−64] The electron convention was used for the electron, which has a gas-phase standard state (25 °C) free energy of −0.87 kcal/mol as calculated by Bartmess using Fermi−Dirac statistics.[65] Using the calculated gas-phase standard free energy of H_2 with the functional and basis employed here, along with the standard free energies of the solvated proton and the gas-phase electron cited above, we obtain the value of 4.30 V for the absolute potential of the normal hydrogen electrode (NHE). A more detailed description of the calculations of pK_a values can be found in the Supporting Information.

Spectroscopic Measurements. All experiments were conducted under an Ar atmosphere. UV−vis spectra were measured on an Agilent 8453 diode-array spectrophotometer. UV−vis spectra of reduced Co^{II} and Co^{I} species of **cat1** were prepared by a direct Na/Hg reduction of the $[\mathbf{Co^{III}}-CH_3CN]^{3+}$ complex in CH_3CN solution under high vacuum using custom-built glassware, at concentrations of ∼1−1.5 × 10^{-4} M. The Na/Hg amalgam was held in a separate compartment (isolated by a glass frit), and the sample was gradually reduced with UV−vis spectral monitoring. The NMR sample of the Co^{I} species was prepared in CD_3CN using custom-built glassware equipped with a Na/Hg chamber, an optical cell, and an NMR tube in the similar way, and the NMR tube was flame-sealed.

UV−vis transient absorption experiments were conducted with a home-built apparatus similar to that described previously,[66] except for the following differences: excitation was provided by an Opotek Vibrant LD 355 II OPO laser (420 nm, 5 ns, 1 mJ/pulse) at 5 Hz. For transient absorption measurements, the sample was probed by a pulsed Xe arc lamp in a 90° beam geometry arrangement, and a Tektronix DPO4032 digital phosphor oscilloscope (350 MHz, 2.5 GS/s) was used to digitize the transient signals from a Hamamatsu R928 PMT detector. The sample was held in a thermostated cell holder, which was maintained at 25.0 ± 0.1 °C. The probe light was filtered through a combination of long-pass and short-pass filters to limit irradiation of the sample. The same setup was used to obtain emission lifetimes, except the sample was not probed with the Xe arc lamp. Transient decays were recorded at individual wavelengths every 10 nm in the range between 320 and 800 nm as the average of 4 pulses.

Electrochemical Measurements. Electrochemical measurements of redox reactions of **cat1** were conducted with a BAS 100b electrochemical analyzer from Bioanalytical Systems. Cyclic voltammograms (CVs) and square-wave voltammograms in aqueous solutions were measured using 50−100 μM solutions of $[\mathbf{Co^{III}}-OH_2]^{3+}$ in water containing 20 mM sodium phosphate (in the 7.0−12.8 pH range) and 0.1 M sodium perchlorate.

A glassy carbon disk (0.28 cm^2) was used as a working electrode, a platinum wire as a counter electrode, and Ag/AgCl (saturated NaCl) as a reference electrode ($E_{Ag/AgCl}$ = 0.203 V vs NHE). The scan rate in CV experiments was varied from 10 to 1000 mV s^{-1}. All potentials in this paper are reported versus NHE. The surface of the electrode was thoroughly polished with diamond paste (0.3 μm), followed by polishing with 0.1 μm Al_2O_3. The polishing with Al_2O_3 was repeated before each scan.

Isotope Exchange Measurements. The measurements of the OH^- ligand exchange in $[\mathbf{Co^{II}}-OH]^{+}$ species were obtained using electrospray ionization (ESI-MS) with a Thermo Finnigan LCQ Advantage instrument. Solutions were prepared under anaerobic conditions inside a glovebox by dissolving $[\mathbf{Co^{II}}-Cl]^{+}$ in basic water and transferring the solution to a gas-tight syringe. ^{18}O-labeled water was deaerated with Ar and placed inside another gas-tight syringe. Both syringes were placed inside a syringe pump and connected to a T-fitting using 100 μm ID capillary tubing. The third port of the T-fitting was connected to the inlet of the ESI unit through a 100 μm ID capillary. The internal volume of the capillary was ∼15 μL, which provided a minimum aging time of ca. 2 s using the highest flow rate available (1 mL/min). Longer aging times were obtained by using capillaries with larger IDs and slower flow rates.

Pulse Radiolysis. Pulse radiolysis studies were performed using the BNL 2 MeV Van de Graaff accelerator using electron pulses (pulse width of 300 ns). A thiocyanate solution (0.01 M KSCN, 0.026 M N_2O) was used for dosimetry taking $G((SCN)_2)$ = 6.13 (G = number of species formed per 100 eV of energy absorbed by the solution) and $\varepsilon_{472\ nm}$ = (7590 ± 230 M^{-1} cm^{-1}). The optical path of the cell was 2 cm. Typical measurements were performed in argon-saturated aqueous solutions containing 0.1 M *tert*-butanol, phosphate buffer if necessary, 150−200 μM of $[\mathbf{Co^{II}}-OH_2]^{2+}$ at 25 °C in the pH range of 3−12.5. Radiolysis of aqueous solutions produces $^{\bullet}OH$, e_{aq}^-, and $H^{\bullet}$ with G values of 2.7, 2.6, and 0.6, respectively. The function of *tert*-butanol is to efficiently scavenge $^{\bullet}OH$ and $^{\bullet}H$ radicals via hydrogen abstraction.[67] The main resulting radical, $^{\bullet}CH_2(COH)(CH_3)_2$, is redox inert. Under such conditions the only remaining redox active intermediate is the strongly reducing e_{aq}^-. Because of the air sensitivity of the complex, all solutions were prepared in a wet glovebox under an Ar atmosphere and transferred to the cell with a minimum exposure to air. The pH of the solution was adjusted by addition of perchloric acid or sodium hydroxide. Experiments to determine the dependence of the kinetics of the decay of the Co^{I} species of **cat1** on the proton source concentration were performed using solutions with phosphate buffer concentration ranging from 0.5 to 10 mM, where sodium perchlorate was used to keep the ionic strength constant. Fresh solutions were used after every four pulses for the kinetics measurements. Quoted rate constants have an error of ca. 15%.

RESULTS

Spectroscopic Properties of cat1. The mass spectrum of the solution of $[\mathbf{Co^{II}}-Cl]^{+}$ (ESI-MS measured in ACN: m/z 461.1, Calcd m/z for $[\mathbf{Co^{II}}-Cl]^{+}$ 461.8) in basic water (pH 12.5) shows rapid substitution of the chloride ligand by an OH^- group and the formation of $[\mathbf{Co^{II}}-OH]^{+}$ (ESI-MS: m/z 442.9, Calcd m/z for $[\mathbf{Co^{II}}-OH]^{+}$ 443.4; Supporting Information, Figure S1). However, the observed signal at m/z 442.9 may correspond either to an ion with the molecular structure $[\mathbf{Co^{II}}-OH]^{+}$ or the five-coordinate $[\mathbf{Co^{II}}-VS]^{2+}$ (VS

DOI: 10.1021/ic5031137
Inorg. Chem. 2015, 54, 4310−4321

= vacant site) with the OH^- associated as a counterion. To differentiate between these two alternatives, a labeling experiment was conducted in which $H_2{}^{18}O$ was added to a solution of $[\mathbf{Co^{II}}{-}Cl]^+$ in $H_2{}^{16}O$ at pH 13. Incorporation of the label into a $[\mathbf{Co^{II}}{-}{}^{18}OH]^+$ ion should result in a new signal at m/z 445.4. The mass spectrum observed immediately (2 s) after mixing equal volumes of $H_2{}^{18}O$ with the solution of $[\mathbf{Co^{II}}{-}OH]^+$ in $H_2{}^{16}O$ indicates the presence of the $[\mathbf{Co^{II}}{-}{}^{16}OH]^+$ ion but not the $[\mathbf{Co^{II}}{-}{}^{18}OH]^+$ ion (Figure S1). This observation is consistent with the presence of $[\mathbf{Co^{II}}{-}OH]^+$ but not the $[\mathbf{Co^{II}}{-}VS]^{2+}$ associated with OH^- in an ion pair. If the latter were the case, an immediate formation of both isotopes in a 50/50 ratio would be expected. The mass spectra of $[\mathbf{Co^{II}}{-}OH]^+$ in the $H_2{}^{16}O/H_2{}^{18}O$ mixture were measured at different delay times from the moment of mixing. A new peak at ca. m/z 445 was observed consistent with the formation of a $[\mathbf{Co^{II}}{-}{}^{18}OH]^+$ species, reaching a plateau at a 50/50 ratio with the $[\mathbf{Co^{II}}{-}{}^{16}OH]^+$ ion as expected from the statistical distribution of the labeled group. The fit of the ratio of both isotopes as a function of time resulted in an estimate of the rate for the ligand exchange k_{ex} = 0.05 s^{-1}. This value is not unreasonable because the rate of water exchange in the $[Cp^*Co(bpy)(OH_2)]^{2+}$ complex was found[68] to be ca. k_{ex} = 0.6 s^{-1}. Here the hydroxide ion is expected to bind more strongly, resulting in a slower exchange.

The subsequent addition of acid to $[\mathbf{Co^{II}}{-}OH]^+$ is expected to produce the aqua complex $[\mathbf{Co^{II}}{-}OH_2]^{2+}$, which was found to be air-sensitive, and all subsequent manipulations with Co^{II} species were conducted under an air-free atmosphere. When an aqueous solution of Co^{II} of **cat1** was titrated from pH 5.1 to 12.5, an increase in the absorption around 300 nm and 350–400 nm and two isosbestic points at 305 and 343 nm were observed (Supporting Information, Figures S2 and S3). The pK_a of ca. 11 of the aqua complex $[\mathbf{Co^{II}}{-}OH_2]^{2+}$ was determined from the least-squares fit of the absorbance versus pH data (Figure S2) and was found to be consistent with the pK_a of ca. 10.7 predicted theoretically and obtained from the pH-dependent electrochemical measurements (vide infra).

The mass spectrum of the solution obtained from the addition of perchloric acid to $[\mathbf{Co^{II}}{-}OH]^+$ (Supporting Information, Figure S4) indicated that the predominant species are $[\mathbf{Co^{II}}{-}ClO_4]^+$ (ESI-MS: m/z 525.1; Calcd m/z for $[\mathbf{Co^{II}}{-}ClO_4]^+$ 525.8) and $[\mathbf{Co^{II}}{-}VS]^{2+}$ (ESI-MS: m/z 213.2; Calcd m/z for $[\mathbf{Co^{II}}{-}VS]^{2+}$ 213.4); however formation of the ion at m/z 213.2 could arise from the fragmentation of the parent ion m/z 525.8. This observation is consistent with a water ligand being weakly bound to the Co^{II} center, which is in agreement with our DFT results (vide infra). The UV–vis spectrum of $[\mathbf{Co^{II}}{-}X]^{n+}$ (X = ClO_4^- or VS) in water did not change over 20 h in the presence of 0.01 M perchloric acid or 0.01 M sodium hydroxide indicating that water-soluble Co^{II} species are stable under acidic and basic anaerobic conditions. The Co^{II} species of **cat1** in water in the presence of >0.1 M sodium hydroxide was found to be unstable.

The CV of $[\mathbf{Co^{III}}{-}CH_3CN]^{3+}$ in CH_3CN reported earlier showed three reversible redox couples: $Co^{III/II}$, $Co^{II/I}$, and $Co^{I/0}$ at potentials 0.35, −0.94, and −1.53 V (vs NHE), respectively, which indicates that the $[\mathbf{Co^{III}}{-}CH_3CN]^{3+}$ could be chemically reduced by a Na amalgam (Na/Hg).[15] Two successive Na/Hg reductions of the initial complex $[\mathbf{Co^{III}}{-}CH_3CN]^{3+}$ in CH_3CN led, respectively, to the quantitative formation of the $[\mathbf{Co^{II}}{-}CH_3CN]^{2+}$ and, more importantly, the $[\mathbf{Co^{I}}{-}VS]^+$ species (Figure 1). The initial yellow solution of $[\mathbf{Co^{III}}{-}CH_3CN]^{3+}$ turns pale orange after a one-electron reduction to form $[\mathbf{Co^{II}}{-}CH_3CN]^{2+}$, with a weak visible absorption. The UV–vis spectrum of the green solution of Co^I exhibits intense absorption in the visible and near-IR regions. UV–vis spectra of the one- and two-electron-reduced DPA-Bpy ligand itself prepared by Na/Hg reduction are distinctly different from the UV–vis spectrum of the two-electron-reduced Co complex (Supporting Information, Figure S5). This suggests that the electron density is mainly localized on the metal center. The Co^I species is extremely stable in air-free dry CH_3CN since no absorption change was observed after several weeks. The ^1H NMR spectrum of the Co^I species of **cat1** in CD_3CN is indicative of a diamagnetic species, indicating that its structure can be assigned as $[\mathbf{Co^{I}}{-}VS]^+$ or $[Co^I(\kappa^4\text{-L})(CD_3CN)]^+$ (Supporting Information, Figure S6).

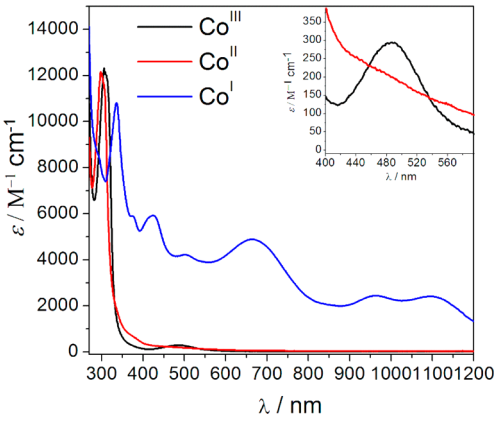

Figure 1. UV–vis absorption spectra of $[\mathbf{Co^{III}}{-}CH_3CN]^{3+}$ in CH_3CN and the $\mathbf{Co^{II}}$ and $\mathbf{Co^{I}}$ species obtained by Na/Hg reduction of $[\mathbf{Co^{III}}{-}CH_3CN]^{3+}$.

Electrochemistry. As was previously reported, bulk electrolysis at −1.4 V (vs NHE) of $[\mathbf{Co^{III}}{-}OH_2]^{3+}$ at neutral pH leads to hydrogen evolution with the activity of 1400 L of H_2 (mol cat)$^{-1}$ h^{-1} (cm^2 Hg)$^{-1}$, or a turnover number (TON) of >300 mol H_2 (mol cat)$^{-1}$, suggesting that the complex is a highly efficient electrocatalyst for proton reduction in neutral aqueous solution.[15] In this work, we explored the redox properties of the complex under electrochemical conditions in more detail.

In 20 mM sodium phosphate buffer at pH 7.0, complex $[\mathbf{Co^{III}}{-}OH]^{2+}$ exhibits a sequence of two redox events centered at 0.15 and −0.90 V (vs NHE), corresponding to $Co^{III/II}$ and $Co^{II/I}$, respectively. The catalytic current for the proton reduction at pH 7.0 occurs at potentials slightly cathodic of −0.9 V and is consistent with Co^I being the highest energy species involved in the electrocatalysis, presumably followed by the formation of $[\mathbf{Co^{III}}{-}H]^{2+}$ (Figure 2). It has been shown by Zhao et al. that when a mercury pool was used as the working electrode, the CV of $[\mathbf{Co^{III}}{-}OH]^{2+}$ in 1.0 M sodium phosphate buffer at pH 7 exhibited strong current at −1.20 V versus NHE concomitant with the formation of H_2 gas.[15]

The pH-dependent cyclic and square-wave voltammograms of $[\mathbf{Co^{III}}{-}OH]^{2+}$ were measured in 20 mM phosphate buffer in the pH range from 7.0 to 12.8 with a glassy carbon working electrode (Supporting Information, Figure S7). The resulting Pourbaix diagram is shown in Figure 3. On the basis of the previous studies, the pK_a of $[\mathbf{Co^{III}}{-}OH_2]^{3+}$ was found to be ca. 5, indicating that the starting material is $[\mathbf{Co^{III}}{-}OH]^{2+}$ in the entire pH range used in this work.

DOI: 10.1021/ic5031137
Inorg. Chem. 2015, 54, 4310–4321

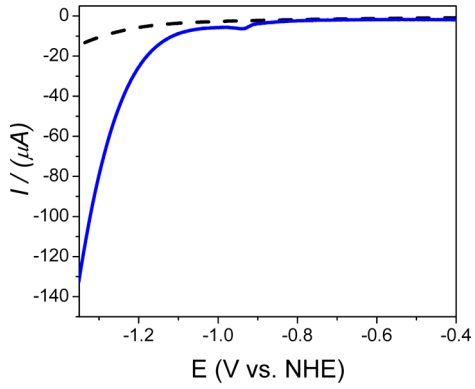

Figure 2. CVs of 20 mM sodium phosphate buffer solution, 0.1 M sodium perchlorate, at pH 8.0 in the presence (blue line) and absence (dotted line) of 50 μM $[\mathbf{Co^{III}}-OH]^{2+}$. Scan rate, 50 mV/s; working electrode: glassy carbon, counter electrode: Pt, reference electrode: Ag/AgCl.

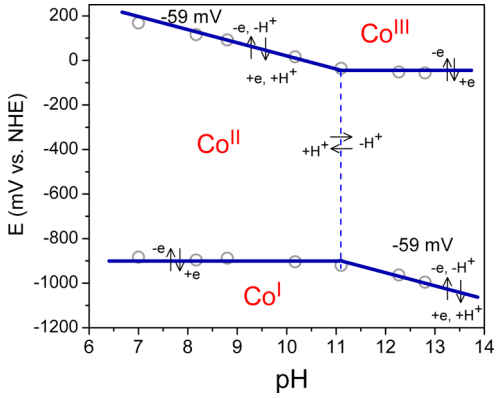

Figure 3. pH-dependent electrochemistry of $[\mathbf{Co^{III}}-OH]^{2+}$ in 20 mM phosphate buffer, 0.1 M sodium perchlorate obtained from square-wave voltammograms performed by scans in a negative direction from 300 to −1200 mV.

A reversible $Co^{III/II}$ wave was observed at +0.15 V in a pH 7.0 phosphate buffer (Supporting Information, Figure S8). Within the pH range 5.0−11.0 this potential shifts linearly with pH with a slope of −59 mV/pH, indicating a proton-coupled electron-transfer process, while above pH 11.0 the reduction of the $[\mathbf{Co^{III}}-OH]^{2+}$ is pH-independent. The Pourbaix diagram indicates that the pK_a of the one-electron-reduced species, $[\mathbf{Co^{II}}-OH_2]^{2+}$, is ∼11. That matches well the pK_a determined independently by UV−vis titration (Figure S2). A second reduction assigned as Co^{II}/Co^{I} in the Pourbaix diagram was found to be pH-independent over a range of pH 7.0−11.0, and therefore, a proton transfer is not involved in this process. Above pH 11.0, the Co^{II}/Co^{I} couple has a slope of −59 mV/pH.

The less negative potential of the $[\mathbf{Co^{III}}-H]^{2+}/[\mathbf{Co^{II}}-H]^{+}$ couple compared to the Co^{II}/Co^{I} couple obtained from our DFT calculations implies that as soon as $[\mathbf{Co^{III}}-H]^{2+}$ is produced, it is converted to $[\mathbf{Co^{II}}-H]^{+}$ and reaction becomes catalytic. Thus, transient methods, for example, pulse radiolysis, are required to observe the $[\mathbf{Co^{III}}-H]^{2+}$ species, since the amount of reducing equivalents produced in these experiments is limited (vide infra).

Pulse Radiolysis. *Spectral Analysis.* The exposure of aqueous solutions of $[\mathbf{Co^{II}}-OH]^{+}$ to e_{aq}^{-} at pH 12.5 leads initially to the formation of a reduced Co^{I} species with an estimated rate constant of 7×10^9 M^{-1} s^{-1}. Interestingly, the spectrum of the Co^{I} species produced by two-electron reduction of $[\mathbf{Co^{III}}-CH_3CN]^{3+}$ by Na/Hg match fairly well those produced by the one-electron reduction of $[\mathbf{Co^{II}}-OH]^{+}$ obtained in the pulse radiolysis. At pH 12.5, the Co^{I} species decays with the rate of $(1.9 \pm 0.3) \times 10^4$ s^{-1} (Figure 4, red

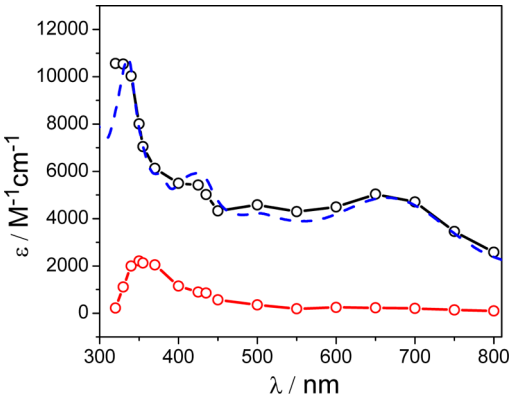

Figure 4. Spectrum of one-electron reduced species measured in pulse radiolysis experiments at pH 12.5 of $[\mathbf{Co^{II}}-OH]^{+}$ 1 μs after the 300 ns pulse of electrons (black line and circles) and the spectrum of the species formed after the decay of the $[\mathbf{Co^{I}}-X]^{+}$ (400 μs after the pulse of electrons) assigned to $[\mathbf{Co^{III}}-H]^{2+}$ (red line and circles). For comparison, the spectrum of the species formed after two-electron reduction of $[\mathbf{Co^{III}}-CH_3CN]^{3+}$ by Na/Hg in acetonitrile (blue dashed line) is also shown.

symbols) concomitantly with the formation of another intermediate with an absorption maximum at 370 nm. The electronic absorption in the 300−450 nm region is similar to those measured for $Co^{III}-H$ of **cat12** and **cat13**,[69] $Co^{III}-Me$ of **cat16**,[37] or predicted by theoretical calculations for $Co^{III}-H$ of **cat15**.[44] In addition, Gray et al. reported that following the proton transfer from the triplet excited state of brominated naphthol to reduced **cat14**, $Co^{III}-H$ was formed with an absorption feature between 380 and 450 nm.[35] Creutz et al. reported spectra of Co-hydrides obtained in pulse radiolysis of cobalt macrocycles **cat12** and **cat13**. These Co-hydrides showed maximum absorbance at 440 nm (ε = 200−500 M^{-1} cm^{-1}) and negligible absorbance above 550 nm.[69] The DFT-calculated spectrum of the $[\mathbf{Co^{III}}-H]^{2+}$ species is qualitatively consistent with the spectra measured in pulse radiolysis and flash photolysis experiments and did not exhibit significant absorption above ca. 300 nm (Supporting Information, Figure S16).

Hamm et al. have recently observed a second-order decay of the Co^{I} species of **cat9**.[48] It was proposed that hydrogen is produced after protonation of $\mathbf{Co^{I}}$ to $\mathbf{Co^{III}}-H$ and the reduction of the latter by excess of $\mathbf{Co^{I}}$ to $\mathbf{Co^{II}}-H$, and finally the protonation of $\mathbf{Co^{II}}-H$. In this work, under conditions of pulse radiolysis, the amount of Co^{I} of **cat1** is limited to the initially available concentration at the beginning of the reaction of ca. 3×10^{-6} M. Even assuming the diffusion-limited rate constant for the disproportionation reaction, the observed rate for the overall disappearance of the Co^{I} species of **cat1** needs to be below 3×10^3 s^{-1} to avoid the buildup of the $\mathbf{Co^{III}}-H$ intermediate. This time scale is over 20 times longer than the time scale observed in our experiment, thus ruling out the possibility of the assignment of the intermediate absorbing at 370 nm to $\mathbf{Co^{II}}-H$. The $^{\bullet}CH_2(COH)(CH_3)_2$ radical formed in

DOI: 10.1021/ic5031137
Inorg. Chem. 2015, 54, 4310−4321

the reaction mixture after initial scavenging of $^{\bullet}OH$ and $^{\bullet}H$ by *tert*-butanol cannot provide additional reducing equivalents owing to its high oxidation potential. However, the reaction between $[\mathbf{Co^{II}}–VS]^+$ and $^{\bullet}CH_2(COH)(CH_3)_2$ forming a radical adduct to the metal center is theoretically possible. For example, the reaction of $^{\bullet}CH_2(COH)(CH_3)_2$ with the N-rac isomer **cat13** was observed but only at very high complex concentration $[CoL^{2+}]$ (1.8 mM) ($k = 1.4 \times 10^6$ M^{-1} s^{-1}).[69] The radical was found to add more rapidly to *N-meso*-CoL^{2+} (**cat12**) ($k = 2 \times 10^7$ M^{-1} s^{-1}) and produced a species with an absorption maximum at 490 nm ($\varepsilon = 150$ M^{-1} cm^{-1}). However, in our case the concentration of the complex $[\mathbf{Co^{II}}–OH]^+$ (150 μM) appears to be too low for such a reaction to take place on the time scale of ca. 400 μs. In addition it was shown by ESI-MS that at basic conditions Co^{II} is six-coordinate $[\mathbf{Co^{II}}–OH]^+$ (Figure S1) with an OH^- exchange rate of ca. 0.05 s^{-1}, which precludes its reaction with the *tert*-butanol radical. All the above arguments favor the assignment of the species absorbing at 370 nm as the key catalytic intermediate $[\mathbf{Co^{III}}–H]^{2+}$.

The transient nature of $[\mathbf{Co^{III}}–H]^{2+}$, especially under equilibrium conditions, for example, during electrochemical reduction of a Co^{III} or Co^{II} parent species, creates a challenge for its experimental characterization, and as a result only a few reports of such intermediates are known.[36,46] While the cobalt hydride species of a Co-polypyridyl-type complex in aqueous solution has been observed earlier,[70] to the best of our knowledge, this is the first report of the UV–vis spectrum of such an intermediate. Gray and co-workers stabilized the reactive intermediate $\mathbf{Co^{III}}–H$ by minimizing the overall reaction free-energy using phosphine ligands around the Co center.[36] This enabled characterization of the $\mathbf{Co^{III}}–H$ and its kinetics by NMR spectroscopy using a Co^{I}(triphos) (triphos = 1,1,1-tris(diphenylphosphinomethyl)ethane) complex.[36] Ott et al. have also recently reported the electrochemical detection of $\mathbf{Co^{III}}–H$ resulting from the protonation of the Co^{I} intermediate of **cat3** under basic aqueous conditions.[46]

Kinetic Analysis. The decay of broad transient absorption features spanning the entire UV–vis region and the formation of species absorbing around 370 nm were assigned to the protonation of the Co^{I} species resulting in the formation of $[\mathbf{Co^{III}}–H]^{2+}$ (Figure 4). The pK_a of $[\mathbf{Co^{III}}–H]^{2+}$ was estimated to be >15 based on the observed protonation under basic conditions where the water (pK_a = 15.7) was the most acidic proton source present in solution at pH 12.5. This value is consistent with the value 13.9 predicted from our DFT calculations. Interestingly, Creutz et al. also determined high pK_a values for **cat12** and **cat13** of >13.9 and 11.8, respectively.[69] Such high basicity of $[\mathbf{Co^{I}}–VS]^+$ is not surprising since under pulse radiolysis conditions the only proton sources present in solution at pH 12.5 are water (pK_a 15.7) and *tert*-butanol (pK_a 16.5),[71] and yet the formation of $[\mathbf{Co^{III}}–H]^{2+}$ was clearly observed on a relatively fast time scale.

It was also found that the decay of the Co^{I} species of **cat1** is independent of the pH (Figure 5 and Supporting Information, Figure S9) over a fairly wide range. At pH 3 the rate constant of the Co^{I} decay as found from the monoexponential fit is $(1.6 \pm 0.3) \times 10^4$ s^{-1}, which is in agreement within experimental error with the rate constant measured at pH 12.5 (Figure 5 and Figure S9). The observed rates show first-order dependence in the concentration of the Co^{I} species of **cat1** (Supporting Information, Figure S10), which further confirms that the order of the reaction is unity. At pH 3 (1 mM $[H_3O^+]$) the observed rate of protonation is expected to be ca. 1×10^6 s^{-1} based on

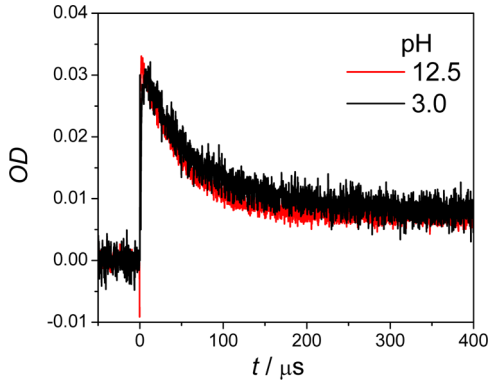

Figure 5. Experimental traces of the 370 nm absorbance decay recorded during pulse radiolysis of $[\mathbf{Co^{II}}–OH]^+$ (200 μM) (pH 12.5, red symbols) or $[\mathbf{Co^{II}}–OH_2]^{2+}$ (200 μM) (pH 3.0, black symbols) complex in deoxygenated aqueous solutions containing 0.1 M *tert*-butanol. The traces indicate the decay of the $\mathbf{Co^{I}}$ species of **cat1** and formation of the final product $[\mathbf{Co^{III}}–H]^{2+}$.

the reported rate constants for the protonation of **cat12** and **cat13** species by H_3O^+, ($k_H^+ = 2.4 \times 10^9$ M^{-1} s^{-1} and 3.1×10^9 M^{-1} s^{-1}, respectively)[69,72] which is 2 orders of magnitude higher compared to the observed rate of the decay of the Co^{I} species of **cat1**.

In addition, the decay of the Co^{I} species of **cat1** was found to occur with the same rate constant within experimental error at pH 7.0 in the presence of 10 mM $H_2PO_4^-/HPO_4^{2-}$ buffer as a proton source, as monitored by absorbance at 650 nm (Figure S9). The predominant proton source at this pH is expected to be $H_2PO_4^-$, which was shown to react with the Co^{I} species of **cat13** with a rate constant of $k_H^+ \approx 1.0 \times 10^8$ M^{-1} s^{-1}.[73] Again, this would result in much higher rates for disappearance of the Co^{I} species of **cat1** than observed in the current study. These experimental results strongly suggest that Co^{I} transformation to $[\mathbf{Co^{III}}–H]^{2+}$ is not a direct, one-step protonation, that the protonation of the Co^{I} species is not the rate-determining step, and some other rate-determining reaction must occur before $[\mathbf{Co^{III}}–H]^{2+}$ is formed (see Discussion Section).

The $[\mathbf{Co^{III}}–H]^{2+}$ generated in pulse radiolysis experiments remains relatively stable on the milliseconds-to-seconds time scale over a wide pH range (Figures S11 and S12), which implies that further reduction of $[\mathbf{Co^{III}}–H]^{2+}$ is required for H_2 evolution (see The Stability of the Metal Hydride Section).

Flash Photolysis. The hydrogen-evolving activity of $[\mathbf{Co^{III}}–OH_2]^{3+}$ has been previously demonstrated in light-driven experiments employing continuous irradiation of aqueous solutions containing $[Ru(bpy)_3]^{2+}$/ascorbate/$[\mathbf{Co^{III}}–OH_2]^{3+}$ with visible light.[15] $[\mathbf{Co^{III}}–OH_2]^{3+}$ was found to generate hydrogen most efficiently in a solution containing 0.5 mM $[Ru(bpy)_3]^{2+}$ and 0.1 M ascorbic acid in 1.0 M acetate buffer at pH 4. Under such conditions, H_2 evolution was observed with a TON of >1600 mol H_2 (mol cat)$^{-1}$ and a TOF of 1500 mol H_2 (mol cat)$^{-1}$ h^{-1}.[15] A follow-up time-resolved flash photolysis study has examined the sequence of kinetic steps involved in the photochemical hydrogen generation using the $[Ru(bpy)_3]^{2+}$/ascorbate/$[\mathbf{Co^{III}}–OH_2]^{3+}$ system.[47]

In the current investigation, the laser flash photolysis technique was used to corroborate results obtained from pulse radiolysis experiments, in particular regarding the intermediate Co^{I} species of **cat1**. Photoexcitation of the $[Ru(bpy)_3]^{2+}$ photosensitizer generates $*[Ru(bpy)_3]^{2+}$, which is reductively quenched by ascorbate as a sacrificial electron

DOI: 10.1021/ic5031137
Inorg. Chem. 2015, 54, 4310–4321

donor (k_q = 1 × 10^7 M^{-1} s^{-1})[47] to produce the reduced photosensitizer $[Ru(bpy)_3]^+$ with a 70% quantum yield (Figures S13 and S14). $[Ru(bpy)_3]^+$ displays a spectroscopic signature with an absorption maximum around 510 nm (Figure S13) and a half-life of ca. 45 μs in the absence of a catalyst.

The addition of the Co^{II} of **cat1** to the flash-quench mixture followed by excitation with 420 nm laser pulses markedly accelerated the disappearance of the initially formed $[Ru(bpy)_3]^+$ species (Supporting Information, Figure S15). This coincided with the generation of a new species possessing a characteristic broad transient between 400 and 800 nm with a maximum around 650 nm (Figure 6). These transient features

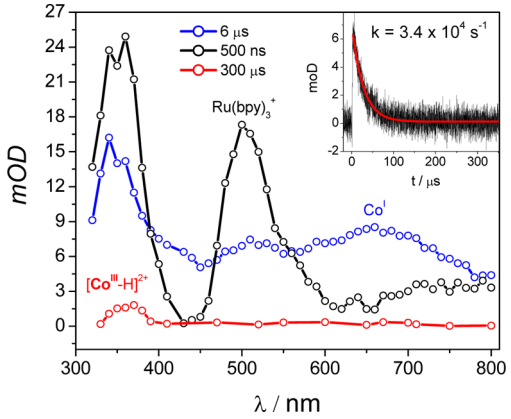

Figure 6. Transient absorption spectra of 150 μM Co^{II} of **cat1**, 30 μM $[Ru(bpy)_3]^{2+}$, and 0.15 M ascorbate following 420 nm photoexcitation in deaerated, 20 mM acetate buffer solution (pH 4). (inset) The transient decay of Co^I at 650 nm.

are similar to those of the Co^I species observed in pulse radiolysis and Na/Hg reduction (Figure S16). The rate constant of the reaction between the reduced photosensitizer and this cobalt catalyst was reported[47] to be 5 × 10^9 M^{-1} s^{-1}, which is similar to that obtained in our experiments. This value is close to the diffusion limit and is the same order of magnitude as reported for the bimolecular electron transfer from the reduced $[Ru(bpy)_3]^+$ to polypridine cobalt complexes of **cat3** and **cat6**.[46,53]

The transient Co^I species subsequently disappeared, accompanied by the formation of the intermediate with the weak absorbance in the region 330−400 nm attributed to the $[\mathbf{Co^{III}}-H]^{2+}$. This observation is in agreement with the results obtained independently by pulse radiolysis (Figure 4). One could argue that the observed absorbance is due to the ascorbyl radical (ε_{360} = 3300 M^{-1} cm^{-1}),[74] which is expected to be formed via very fast deprotonation of the highly acidic ascorbate radical (pK_a = −0.45).[75] Thus, the ascorbyl radical should be present in the solution within the same time scale that Co^I is formed. Its presence would be manifested by the discrepancy between the Co^I spectra obtained in the flash photolysis and Na/Hg reduction in the region 320−400 nm due to hidden absorption from the ascorbyl radical underneath the Co^I. The very good agreement between the spectra of the Co^I species of **cat1** obtained in the flash photolysis and chemical reduction excludes any contribution from the ascorbyl radical. The ascorbyl radical is unstable in aqueous solutions and may decay via several pathways including disproportionation.[75] On the basis of the spectra of Co^I and $[\mathbf{Co^{III}}-H]^{2+}$ determined from the pulse radiolysis studies, the absorbance ratio of $Co^I/[\mathbf{Co^{III}}-H]^{2+}$ at 370 nm corrected for the bleach of Co^{II} was found to be ∼3/1 (Figure 4). The analogous ratio of ca. 4.1/1 was found in flash photolysis studies, indicating that the yield for the formation of $[\mathbf{Co^{III}}-H]^{2+}$ in flash photolysis relative to the yield for the formation of $[\mathbf{Co^{III}}-H]^{2+}$ in pulse radiolysis is ∼0.7. The apparent lifetime of the Co^I species is ∼30 μs (k = 3.4 × 10^4 s^{-1}) for the solution containing 150 μM Co^{II}, 30 μM $[Ru(bpy)_3]^{2+}$, and 0.15 M ascorbate at pH 4.0. This rate constant was determined from single exponential fits of the kinetics measured at 650 nm, where the Co^I species absorbs exclusively (inset, Figure 6). This rate is similar to the rate of disappearance of Co^I in aqueous solutions as determined in pulse radiolysis experiments.

Photogeneration of the Co^I of cat1 and Its Reactivity with Proton Donors in Acetonitrile. The reduced Co^I species of **cat1** can also be produced by continuous irradiation of solutions containing $[Ru(bpy)_3]^{2+}$/1,3-dimethyl-2-phenyl-2,3-dihydro-1*H*-benzo[*d*]imidazole (BIH)/$[\mathbf{Co^{II}}-CH_3CN]^{2+}$ in CH_3CN. It was reported recently that BIH can be used as an efficient two-electron donor.[76] Unlike TEA or TEOA, BIH can efficiently reduce $*[Ru(bpy)_3]^{2+}$ with rates close to the diffusion limit. The photogenerated $[Ru(bpy)_3]^+$ is stable under these reaction conditions, indicating that BIH acts as an efficient sacrificial reagent and that back electron transfer does not take place. The addition of the catalyst $[\mathbf{Co^{II}}-CH_3CN]^{2+}$ to the flash-quench mixture followed by excitation with 420 nm laser pulses markedly accelerated the disappearance of the initially formed $[Ru(bpy)_3]^+$ species, which coincided with the formation of the Co^I species with a maximum absorption at 650 nm (Supporting Information, Figure S17). The rate constant of the reaction between the reduced photosensitizer and $[\mathbf{Co^{II}}-CH_3CN]^{2+}$ was found to be 8.1 × 10^7 M^{-1} s^{-1} (inset, Figure S17).

Steady-state irradiation of the reaction mixture containing $[Ru(bpy)_3]^{2+}$/BIH/$[\mathbf{Co^{II}}-CH_3CN]^{2+}$ in CH_3CN with an argon ion laser (λ_{exc} = 476 nm) for 5 min led to the quantitative formation of the Co^I species (Supporting Information, Figure S18). In the absence of a proton source the Co^I species is very stable, but the addition of only a few equivalents of relatively weak acetic acid (pK_a = 22.3 in CH_3CN)[77] to the solution of the photogenerated Co^I species in CH_3CN led to the regeneration of the starting complex $[\mathbf{Co^{II}}-CH_3CN]^{2+}$ within a few seconds. Even the addition of 0.1 M water led to the protonation of the Co^I species within a few minutes, which confirms the high basicity of the Co^I species of **cat1**. It was recently reported that an electrogenerated Co^I tetraaza-macrocyclic **cat11** is stable after addition of acetic acid. Only after addition of the stronger trifluoroacetic acid (pK_a = 12.7 in CH_3CN),[77] the slow recovery of the Co^{II} species was monitored (34% after 20 min).[52] The higher basicity of the investigated Co^I species compared to the **cat11** complex can be explained based on the comparison of the reduction potential of the $Co^{II/I}$ couple. The reduction potential of the **cat11** complex is less negative (−0.62 V vs NHE in water)[77] than the $Co^{II/I}$ species studied in this work (−0.9 V vs NHE in water).

Density Functional Theory Results. The energetics of the key intermediates proposed to be involved in the catalytic proton reduction mediated by **cat1** were predicted based on DFT calculations. While DFT calculations predict that Co^{III} species are six-coordinate (the sixth ligand is H_2O or OH^-), they also predict that the binding of the solvent ligand weakens significantly upon reduction, making five-coordinate $[\mathbf{Co^{II}}-VS]^{2+}$ and $[\mathbf{Co^{I}}-VS]^{+}$ the lowest-energy species (Supporting

DOI: 10.1021/ic5031137
Inorg. Chem. 2015, 54, 4310−4321

Information, Table S1). Surprisingly, another set of five-coordinate species was identified by DFT with the aqua or hydroxyl ligand still attached to the cobalt center, but with the detachment of one of the pyridine rings of the DPA-Bpy ligand from the metal (Figure S19). In the case of the aqua complex, the complex is stabilized by a hydrogen bond between a proton from the aqua ligand and the detached N-site. We denote those as $[Co(\kappa^4\text{-L})(OH_2)]^{n+}$, and their relative energies are also shown in Table S1. The calculations indicate that the loss of the aqua ligand is more energetically favorable than κ^4-coordination with retention of the aqua ligand.

Using calculated free energies of cobalt complexes (Table S1) and the values of the standard free energies of H_2O (liquid), the solvated proton, the gas-phase electron, and the value of the absolute potential of the normal hydrogen electrode (NHE), a Pourbaix diagram can be constructed[78] for various redox and acid–base states of **cat1** (Figure 7).

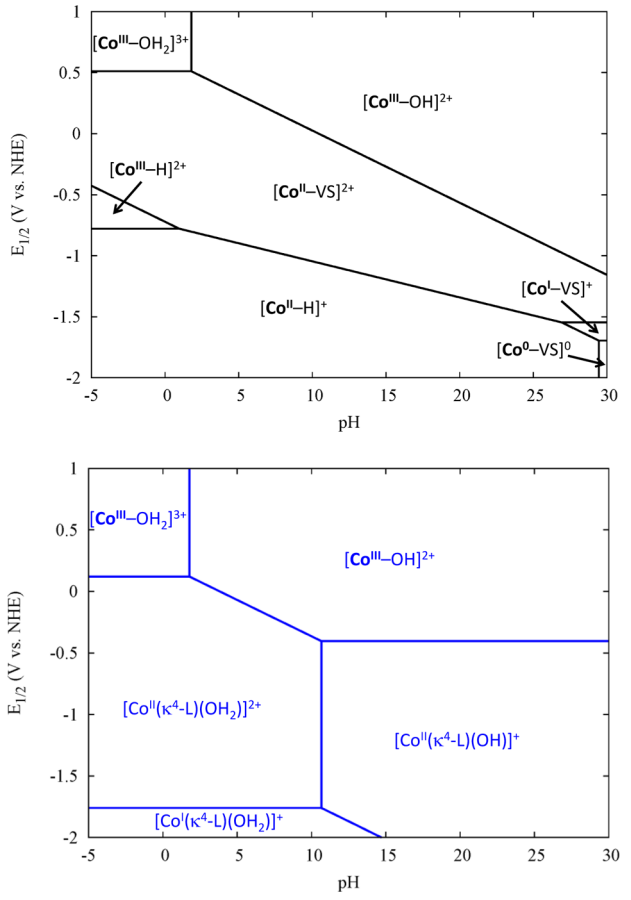

Figure 7. DFT-calculated Pourbaix diagrams of **cat1** assuming that the first and second reductions of the $[\mathbf{Co^{III}}–OH_2]^{3+}$ result in (upper) solvent ligand loss and (lower) the formation of $[Co(\kappa^4\text{-L})(OH_2)]^{n+}$, n = 2, 1.

Interestingly, while the Pourbaix diagram constructed using theoretically predicted energetics for $[\mathbf{Co^{II}}–VS]^{2+}$ and $[\mathbf{Co^{I}}–VS]^{+}$ species (Figure 7, upper) is distinctly different from the experimental results (Figure 3), the DFT-calculated diagram involving $[Co(\kappa^4\text{-L})(OH_2)]^{n+}$ (Figure 7, lower) is very similar to the experiment. This similarity of the Pourbaix diagrams indicates that $[Co^{I}(\kappa^4\text{-L})(OH_2)]^{+}$ is present in the solution in pulse radiolysis experiments.

The calculations also predict that even though the pK_a of $[\mathbf{Co^{III}}–H]^{2+}$ is 13.94, it does not exist on the Pourbaix diagram above pH 1.79 because the two-electron, one-proton PCET reduction of $[\mathbf{Co^{II}}–VS]^{2+}$ (which, in turn, is predicted to be more stable than $[\mathbf{Co^{II}}–OH_2]^{2+}$ or $[\mathbf{Co^{II}}–OH]^{+}$) forms $[\mathbf{Co^{II}}–H]^{+}$ from pH 1.79 to pH ≈ 27.

The Stability of the Metal Hydride. $[\mathbf{Co^{III}}–H]^{2+}$ generated in pulse radiolysis was found to be stable at pH 12.5 for at least 5 s (Supporting Information, Figure S11). The observed stability of the $[\mathbf{Co^{III}}–H]^{2+}$ suggests that hydrogen production is unlikely to occur via the reaction of two $[\mathbf{Co^{III}}–H]^{2+}$ species in a bimolecular fashion. It also points to the fact that water is not strong enough to further protonate $[\mathbf{Co^{III}}–H]^{2+}$ to produce hydrogen in a heterolytic pathway. This is consistent with earlier studies by Ott and co-workers who found that the $\mathbf{Co^{III}}$–H intermediate of **cat3** was sufficiently stable under basic conditions to accumulate during voltammetric scans.[46] Additionally, pulse radiolysis experiments allowed us to probe the stability of $[\mathbf{Co^{III}}–H]^{2+}$ at lower pH, at which electrochemical measurements under cathodic bias are usually complicated by proton reduction at the electrode. Under mildly acidic conditions, that is, pH 3, the disappearance of the absorbance at 370 nm attributed to $[\mathbf{Co^{III}}–H]^{2+}$ was not observed on the 50 ms time scale (Supporting Information, Figure S12), indicating that the rate constant for its disappearance is below 2×10^1 s^{-1}. The slow disappearance of the $[\mathbf{Co^{III}}–H]^{2+}$ species might be related to the necessity of its further reduction to $[\mathbf{Co^{II}}–H]^{+}$.

DISCUSSION

The mechanism of proton reduction catalyzed by various cobalt coordination complexes has been extensively studied in the past and, in general, follows the pathway shown in Scheme 1.

Scheme 1. Proposed Reaction Pathways for H_2 Evolution Catalyzed by the cat1 in Water[a]

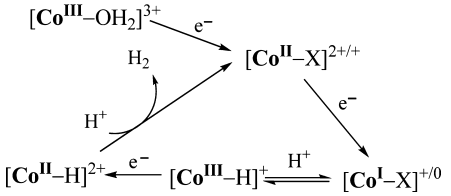

[a]Depending on conditions, X can be a water molecule, hydroxide, or other anion present in the solution.

Despite significant recent progress in the understanding of the reactivity of Co-based proton reduction catalysts, the properties of certain reaction intermediates such as Co^{I} and Co^{III}–H are still relatively unknown owing to their transient nature, especially in aqueous media. The crucial step for the catalysis, that is, the protonation of the Co^{I} to Co^{III}–H species can occur only after dissociation of the monodentate ligand (X) from the inner coordination sphere. Alternatively, protonation of Co^{I} as suggested recently by Wang[22] can take place after detachment of one of the pyridines of the pentadentate ligand. In this work, we focus on the properties of several reaction intermediates, such as $[\mathbf{Co^{II}}–X]^{2+/+}$, $[\mathbf{Co^{I}}–X]^{+/0}$, and $[\mathbf{Co^{III}}–H]^{2+}$, as well as transformation of $[\mathbf{Co^{I}}–X]^{+/0}$ to $[\mathbf{Co^{III}}–H]^{2+}$.

Most cobalt complexes used as hydrogen production catalysts, including **cat1** studied in this work, are six-coordinate systems in their oxidized form and rely on the loss of one of the

DOI: 10.1021/ic5031137
Inorg. Chem. 2015, 54, 4310–4321

ligands to accommodate an incoming proton leading to the formation of a cobalt hydride intermediate.

Complexes with the cobalt oxidation state 2+ were reported to be either five-coordinate or six-coordinate. Peters et al. obtained the crystal structure for the six-coordinate complex of **cat16** in which the Co^{II} ion is ligated by a planar difluoroboryl–diglyoxime ligand and by two trans-oriented acetonitrile molecules.[8] On the other hand, Alberto et al. reported the crystal structure of **cat9** that had strongly distorted octahedral coordination geometry, consisting of a pentacoordinate TPY–OH-bromide complex with the bromide counteranion as far as 2.79 Å from the Co^{II} center.[79] One or more ligands in the cobalt coordination sphere of known catalysts are halide or solvent species, and they are released upon crossing the $Co^{III/II}$ couple resulting in the formation of a pentacoordinate intermediate.[7,8] If the rate of the ligand loss is faster than or comparable to the rate of electron transfer at the electrode, the reduction wave will appear as an irreversible process corresponding to the electrochemical mechanism. For example, Artero et al. showed that for **cat14** the Co^{III}/Co^{II} couple appeared irreversible in the scanning range of 20–2000 mV s^{-1}. On the basis of simulations of electrochemical data, the rate of halide ligand loss was estimated to be in the range from 1×10^5 to 1×10^9 s^{-1} depending on the substitution on the pyridine ligand.[7] In our study the reduction of $[\mathbf{Co^{III}}–Cl]^{2+}$ in acetonitrile appears as a reversible one-electron process, indicating that the $[\mathbf{Co^{II}}–Cl]^{+}$ is relatively stable toward the chloride loss.[15] The presence of the six-coordinate complex of $[\mathbf{Co^{II}}–Cl]^{+}$ in acetonitrile was confirmed in the ESI-MS. Even the following $Co^{II/I}$ reduction in CH_3CN appears as a reversible or quasi-reversible couple, pointing to fairly strong binding of the chloride ligand to the metal center. However, the redox behavior of solvent-bound species, for example, $[\mathbf{Co^{III}}–OH_2]^{3+}$, is of higher interest because these species are more likely to be present under catalytic conditions. The first redox couple corresponding to the reduction of $[\mathbf{Co^{III}}–OH_2]^{3+}$ in water appears as a one-electron reversible wave (Supporting Information, Figure S8); however, the rapid loss of the aqua ligand cannot be excluded since water is present in large excess and can bind rapidly on the anodic scan. The chemically prepared $[\mathbf{Co^{II}}–Cl]^{2+}$ upon dissolution in basic water produces six-coordinate $[\mathbf{Co^{II}}–OH]^{+}$, which can be clearly observed by, for example, mass spectroscopy (Supporting Information, Figure S1). The isotope labeling experiments confirm the molecular nature of the observed $[\mathbf{Co^{II}}–OH]^{+}$ ion (Figure S1) and provide an estimate for the rate of loss of the hydroxo ligand, which was found to be ~0.05 s^{-1}. The observed rate falls within the range of water exchange rates observed for other Co coordination complexes, for example, $[Cp^*Co(bpy)(OH_2)]^{2+}$ (k_{ex} = 0.6 s^{-1}).[68]

However, upon acidification of a solution of $[\mathbf{Co^{II}}–OH]^{2+}$, the resulting species identified by ESI-MS are consistent with $[\mathbf{Co^{II}}–ClO_4]^{+}$ and $[\mathbf{Co^{II}}–VS]^{2+}$. This observation indicates that the binding of the aqua ligand is either very weak or unfavorable, leading to facile anation. This observation is consistent with $[\mathbf{Co^{II}}–VS]^{2+}$ being the most stable structure predicted by DFT compared to, for example, $[Co^{II}(\kappa^4\text{-}L)(OH_2)]^{2+}$; however, the energy difference possibly lies within the calculation error considering substantial uncertainties in the solvation energies. The anation of Co^{II} with acetate was observed previously for the case of **cat8** in acetonitrile, leading to the appearance of new redox features pertinent to the redox chemistry of the Co-acetate complex.[80] However, in the case of $[\mathbf{Co^{II}}–ClO_4]^{+}$ the anion binding appears to be too weak to play any significant role in the redox behavior of the cobalt complex.

The observed acid–base reactivity of the Co^{II} species (Supporting Information, Figure S2) can be explained by either simple acid–base equilibrium between $[\mathbf{Co^{II}}–OH_2]^{2+}$ and $[\mathbf{Co^{II}}–OH]^{+}$ or a more complex reaction pathway that involves aqua ligand loss.

$$[\mathbf{Co^{II}}–OH]^{+} + H^{+} \longrightarrow [\mathbf{Co^{II}}–OH_2]^{2+} \longrightarrow [\mathbf{Co^{II}}–VS]^{2+} + H_2O$$

The second reduction corresponding to the $Co^{II/I}$ process appears again as a quasi-reversible couple during the electrochemical experiment (Supporting Information, Figure S8). The −59 mV/pH slope in the basic region (above pH 11) of the Pourbaix diagram is indicative of the $[Co^{II}(\kappa^4\text{-}L)–OH]^{+}$/$[Co^{I}(\kappa^4\text{-}L)(OH_2)]^{+}$ transformation (Figure 3), while the pH independent part (below pH 11) can correspond either to $[\mathbf{Co^{II}}–VS]^{+}$/$[\mathbf{Co^{I}}–VS]^{+}$ or $[\mathbf{Co^{II}}–OH_2]^{+}$/$[Co^{I}(\kappa^4\text{-}L)(OH_2)]^{+}$ reactions. However irrelevant it may be to the formation pathway, the $[Co^{I}(\kappa^4\text{-}L)(OH_2)]^{+}$ species is expected to bind water very weakly, leading to the formation of $[\mathbf{Co^{I}}–VS]^{+}$. For example, the crystal structure of the $1e^-$ reduced **cat16** contains a five-coordinate cobalt(I) center in a distorted square-pyramidal ligand environment.[8] The basicity of $[\mathbf{Co^{I}}–VS]^{+}$ was determined from pulse radiolysis measurements and the pK_a of the conjugate acid $[\mathbf{Co^{III}}–H]^{2+}$ was estimated to be ≥15.7. This appears to be higher than those of most cobaloxime compounds. Such a high pK_a value for a Co^{III}-hydride species is unusual but not unprecedented. For example, a pK_a > 13.9 was reported for **cat12**.[69] This high basicity of the $[\mathbf{Co^{I}}–VS]^{+}$ species is consistent with the relatively negative reduction potential of the $\mathbf{Co^{II/I}}$ couple. Theoretical studies by Hammes–Schiffer et al. demonstrated that the pK_a values of cobaloxime-based cobalt hydrides in CH_3CN increased linearly as the $Co^{II/I}$ reduction potentials became more negative.[43] The $Co^{II/I}$ potential of **cat1** ($E(Co^{II/I})$ = −0.9 vs NHE) is more negative than the corresponding reduction potential for some highly active cobaloximes, and thus higher basicity of Co^{I} is expected. As a consequence, the catalytic activity of cobalt catalysts will depend greatly on the acid pK_a values. It was reported that complexes with more negative reduction potentials can catalyze proton reduction with weaker acids at higher rates than those with more positive reduction potentials. For example, Peters et al. reported that the complex with the most negative $Co^{II/I}$ reduction potential, **cat15**, mediated H_2 evolution in CH_3CN using the weak acid CF_3COOH (pK_a = 12.7; $E(Co^{II/I})$ = −0.31 V vs NHE),[8] whereas a complex with more positive potentials, **cat16** ($E(Co^{II/I})$ = −0.04 V vs NHE), catalyzes H_2 evolution only in the presence of TsOH (pK_a = 8.0), and the complex with the most positive potentials, $[Co(Tim^{Me/Ph})(CH_3CN)_2]^{3+}$ (Tim = [14]-tetraene-N_4; $E(Co^{II/I})$ = 0.04 V vs NHE) required an even stronger acid, such as $HBF_4{\cdot}Et_2O$ (pK_a = 0.1).[8] The ability of $[\mathbf{Co^{I}}–VS]^{+}$ to be protonated by very weak acids, such as water, makes it well-suited for proton reduction systems that operate under neutral or basic conditions.

The very high pK_a of the $[\mathbf{Co^{III}}–H]^{2+}$ species creates tremendous driving force for the protonation reaction (e.g., −19 kcal/mol assuming pK_a 14), which would result in very rapid formation of the $[\mathbf{Co^{III}}–H]^{2+}$ intermediate. In such case, the $Co^{II/I}$ couple should exhibit a pH dependence (−59 mV/

DOI: 10.1021/ic5031137
Inorg. Chem. 2015, 54, 4310–4321

pH at pH < 11 and −118 mV/pH above pH 11) according to an electrochemical mechanism in which electrochemical step is followed by the rapid chemical change (eqs 1 and 2).[81]

$$[\mathbf{Co^{II}} - OH]^{+} + 2H^{+} + e^{-} \rightarrow [\mathbf{Co^{III}} - H]^{2+} + H_2O \quad (1)$$

$$[\mathbf{Co^{II}} - VS]^{2+} + H^{+} + e^{-} \rightarrow [\mathbf{Co^{III}} - H]^{2} \quad (2)$$

The observed pH dependence of the $Co^{II/I}$ couple does not match the predicted behavior on the time scale of the electrochemical measurements (scan rate down to 10 mV/s). However, electrochemical results are more consistent with an electrochemical-chemical-chemical (ECC) mechanism, with the first chemical step being pH-independent and rate-limiting and the second chemical step being the reaction with a proton source. Rate constants for protonation of the Co^{I} form of complexes **cat12** and **cat13** by various proton donors are relatively high (k_{H3O^+} = 3 × 10^9 M^{-1} s^{-1}; k_{H2PO4^-} = 1 × 10^8 M^{-1} s^{-1}; $k_{H2PO4^{2-}}$ = 1 × 10^5 M^{-1} s^{-1}), and the protonation by the water molecule can be as fast as 5 × 10^5 M^{-1} s^{-1}. This implies that under electrochemical conditions ([phosphate] = 20 mM; $[H_2O]$ = 55 M) the rate of the first chemical step needs to be below ca. 1 × 10^5 s^{-1} to be rate limiting, thus eliminating the dependence of the reduction couple on the pH.

The kinetics evidence from the pulse radiolysis suggest that the Co^{I} species of **cat1** must undergo some structural change prior to accepting the proton, and this transformation represents the kinetic limiting step in the overall formation of the $[\mathbf{Co^{III}}–H]^{2+}$ species. The origin of such a slow kinetic step might be (i) the removal of a solvent ligand bound to the metal center or (ii) significant structural reorganization of the metal complex and surrounding solvent resulting in a high free energy of activation (Supporting Information, Figure S20). The first scenario would involve aqua ligand loss from the $[Co^{I}(\kappa^4\text{-}L)(OH_2)]^{+}$ species and the formation of the corresponding $[\mathbf{Co^{I}}–VS]^{+}$ (Scheme 2). While the $[\mathbf{Co^{I}}–VS]^{+}$ species is more

Scheme 2. Proposed Reaction Pathways for Protonation Step of the Co^{I} Species of cat1

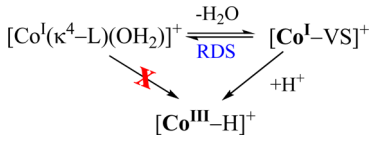

stable by ca. 14 kcal/mol based on DFT calculations, the kinetic barrier for such transformation can be significant due to the structural reorganization. On the other hand, the reorganization energy for the protonation of $[\mathbf{Co^{I}}–VS]^{+}$ to form $[\mathbf{Co^{III}}–H]^{2+}$ can be significant, also contributing to the kinetic barrier. The inner-sphere reorganization energy can be estimated from DFT calculations,[82] while outer-sphere reorganization energy can be calculated using the solvent polarization model[83] (see Supporting Information for details). The obtained values for λ_{in} and λ_{out} are 1.02 and 1.1 eV, respectively, which combined present a significant contribution to the free energy barrier for the protonation reaction.

Since it appears that the experimental Pourbaix diagram reflects Co^{II} intermediates that are kinetically favored but thermodynamically less stable and that solvent coordination to the Co^{I} intermediates is expected to be even weaker, it is tempting to explore the structure of a theoretical Pourbaix diagram in which reduction of the $Co^{II/I}$ couples switches back to the thermodynamically favored five-coordinate κ^5-L species (i.e., $[Co^{II}(\kappa^4\text{-}L)(OH_2)]/[Co^{I}(\kappa^5\text{-}L)(VS)]$ couples). Such a diagram, in which the topology of these couples differs from that of the purely thermodynamic one, because of the intervening Co(II) species is shown in Supporting Information, Figure S21 (and associated Latimer–Frost diagram in Figure S22), and is generally consistent with the experimental results presented in this work.

The $[\mathbf{Co^{III}}–H]^{2+}$ intermediate appears to be relatively stable in the absence of additional reducing equivalents, for example, as generated in pulse radiolysis experiments. However, if produced electrochemically, it does not accumulate at the electrode owing to its less cathodic potential compared to the $Co^{II/I}$ couple, undergoes further reduction to $[\mathbf{Co^{II}}–H]^{+}$, and after an additional protonation reaction becomes catalytic.

CONCLUSION

The redox and acid/base transformations of the cobalt-based molecular hydrogen evolution catalyst $[(DPA\text{-}Bpy)\text{-}Co^{III}(OH_2)]^{3+}$ were studied in aqueous solutions using electrochemical and transient methods, including pulse radiolysis and laser flash photolysis. The experimental results were also corroborated by DFT calculations. It was found that, while the water ligand is strongly coordinated to the metal center in the oxidation state 3+, one-electron reduction of the complex to form Co^{II} species results in weakening the Co–O bond. The $[\mathbf{Co^{II}}–OH]^{+}$ species was found to be relatively stable under basic conditions with the rate of the OH^{-} exchange of ca. 0.05 s^{-1}. Both experimental and theoretical results suggest that the $[\mathbf{Co^{II}}–OH_2]^{2+}$ species is not stable compared to $[\mathbf{Co^{II}}–VS]^{2+}$; however, the solvent coordination can be preserved in $[Co^{II}(\kappa^4\text{-}L)(OH_2)]^{2+}$ as predicted by DFT calculations. An additional reduction of the complex produces a Co^{I} species in which the solvent binding weakens further to favor a five-coordinate $[\mathbf{Co^{I}}–VS]^{+}$ species. Intriguingly, the existence of the transient $[Co^{I}(\kappa^4\text{-}L)(OH_2)]^{+}$ species (with water retained and one pyridine losing its coordination with the Co center) was predicted by DFT calculations, and its formation was found to be consistent with the experimental Pourbaix diagram. The formation of the Co^{I} species coincides with the onset of catalytic current on the electrochemistry time scale, indicating that this is the most energetic species in the proton reduction catalytic cycle. The protonation of the Co^{I} species was observed in the entire pH range up to 12.5, suggesting that the pK_a of $[\mathbf{Co^{III}}–H]^{2+}$ is >15.7. This finding is corroborated by the DFT-calculated value of 13.94. It was also found that the decay of the Co^{I} species is independent of the pH over a fairly wide range. This kinetics result indicates that the Co^{I} species must undergo some structural change prior to accepting the proton, and this transformation represents the kinetics limiting step in the overall formation of the $[\mathbf{Co^{III}}–H]^{2+}$. We suggest that the origin of such a slow kinetics step may be slow water ligand loss from the transiently formed $[Co^{I}(\kappa^4\text{-}L)(OH_2)]^{+}$ intermediate. Alternatively, significant inner-sphere and solvent reorganization energies may contribute to the slow protonation of $[\mathbf{Co^{I}}–VS]^{+}$ to form $[\mathbf{Co^{III}}–H]^{2+}$. The value of λ_{in} = 1.02 eV was estimated from DFT calculations, while λ_{out} = 1.1 eV was obtained on the basis of solvent polarization model. The $[\mathbf{Co^{III}}–H]^{2+}$ species produced in pulse radiolysis experiments was found to be stable for several seconds under basic conditions. On the basis of the observed stability of the Co^{III}–hydride species it was also concluded that under electrochemical conditions hydrogen

DOI: 10.1021/ic5031137
Inorg. Chem. 2015, 54, 4310–4321

production does not occur via the reaction of two Co^{III}–hydrides in a bimolecular fashion.

■ ASSOCIATED CONTENT

Supporting Information

ESI-MS spectra, plots of acid–base titration data, UV–vis spectra, ^1H NMR spectra, cyclic and square-wave voltammograms, log–log plots of kinetics data, experimental traces of absorbance decay, transient absorption spectra, kinetic traces, calculation of pK_a values, tabulated calculated relative standard free energies and reduction potentials, illustrated DFT structures, "hybrid Pourbaix" diagram, calculated inner- and outer-sphere reorganization energies. This material is available free of charge via the Internet at http://pubs.acs.org.

■ AUTHOR INFORMATION

Corresponding Authors

*E-mail: alewand@amu.edu.pl. (A.L.-A.)
*E-mail: dmitriyp@bnl.gov. (D.E.P.)

Present Address

§Faculty of Chemistry, Adam Mickiewicz University, Umultowska 89b, 61614, Poznan, Poland.

Notes

The authors declare no competing financial interest.

■ ACKNOWLEDGMENTS

Dr. Y. Matsubara is acknowledged for providing a BIH sample. The work at Brookhaven National Laboratory (BNL) was performed under Contract No. DE-SC00112704 with the U.S. Department of Energy and supported by its Division of Chemical Sciences, Geosciences, & Biosciences, Office of Basic Energy Sciences. Accelerator Center for Energy Research (ACER) at BNL is acknowledged for providing access to Van de Graaff pulse radiolysis facility. X.Z. acknowledges the financial support from NSF EPS 1004083 and CHE 1352036.

■ REFERENCES

(1) Gray, H. B. *Nat. Chem.* **2009**, *1*, 112–112.
(2) Lewis, N. S.; Nocera, D. G. *Proc. Natl. Acad. Sci. U. S. A.* **2006**, *103*, 15729–15735.
(3) Artero, V.; Fontecave, M. *Coord. Chem. Rev.* **2005**, *249*, 1518–1535.
(4) Eckenhoff, W. T.; Eisenberg, R. *Dalton Trans.* **2012**, *41*, 13004–13021.
(5) Dempsey, J. L.; Brunschwig, B. S.; Winkler, J. R.; Gray, H. B. *Acc. Chem. Res.* **2009**, *42*, 1995–2004.
(6) Hu, X.; Cossairt, B. M.; Brunschwig, B. S.; Lewis, N. S.; Peters, J. C. *Chem. Commun.* **2005**, 4723–4725.
(7) Razavet, M.; Artero, V.; Fontecave, M. *Inorg. Chem.* **2005**, *44*, 4786–4795.
(8) Hu, X.; Brunschwig, B. S.; Peters, J. C. *J. Am. Chem. Soc.* **2007**, *129*, 8988–8998.
(9) Hawecker, J.; Lehn, J. M.; Ziessel, R. *Nouv. J. Chem.* **1983**, *7*, 271–277.
(10) Du, P.; Knowles, K.; Eisenberg, R. *J. Am. Chem. Soc.* **2008**, *130*, 12576–12577.
(11) Du, P.; Schneider, J.; Luo, G.; Brennessel, W. W.; Eisenberg, R. *Inorg. Chem.* **2009**, *48*, 4952–4962.
(12) McCormick, T. M.; Calitree, B. D.; Orchard, A.; Kraut, N. D.; Bright, F. V.; Detty, M. R.; Eisenberg, R. *J. Am. Chem. Soc.* **2010**, *132*, 15480–15483.
(13) Khnayzer, R. S.; Thoi, V. S.; Nippe, M.; King, A. E.; Jurss, J. W.; El Roz, K. A.; Long, J. R.; Chang, C. J.; Castellano, F. N. *Energy Environ. Sci.* **2014**, *7*, 1477–1488.
(14) Nippe, M.; Khnayzer, R. S.; Panetier, J. A.; Zee, D. Z.; Olaiya, B. S.; Head-Gordon, M.; Chang, C. J.; Castellano, F. N.; Long, J. R. *Chem. Sci.* **2013**, *4*, 3934–3945.
(15) Singh, W. M.; Baine, T.; Kudo, S.; Tian, S.; Ma, X. A. N.; Zhou, H.; DeYonker, N. J.; Pham, T. C.; Bollinger, J. C.; Baker, D. L.; Yan, B.; Webster, C. E.; Zhao, X. *Angew. Chem., Int. Ed.* **2012**, *51*, 5941–5944.
(16) Sun, Y.; Bigi, J. P.; Piro, N. A.; Tang, M. L.; Long, J. R.; Chang, C. J. *J. Am. Chem. Soc.* **2011**, *133*, 9212–9215.
(17) Tong, L.; Zong, R.; Thummel, R. P. *J. Am. Chem. Soc.* **2014**, *136*, 4881–4884.
(18) Zhang, P.; Wang, M.; Gloaguen, F.; Chen, L.; Quentel, F.; Sun, L. *Chem. Commun.* **2013**, *49*, 9455–9457.
(19) Brown, G. M.; Brunschwig, B. S.; Creutz, C.; Endicott, J. F.; Sutin, N. *J. Am. Chem. Soc.* **1979**, *101*, 1298–1300.
(20) Krishnan, C. V.; Sutin, N. *J. Am. Chem. Soc.* **1981**, *103*, 2141–2142.
(21) Krishnan, C. V.; Creutz, C.; Mahajan, D.; Schwarz, H. A.; Sutin, N. *Isr. J. Chem.* **1982**, *22*, 98–106.
(22) Xie, J.; Zhou, Q.; Li, C.; Wang, W.; Hou, Y.; Zhang, B.; Wang, X. *Chem. Commun.* **2014**, *50*, 6520–6522.
(23) Kilgore, U. J.; Stewart, M. P.; Helm, M. L.; Dougherty, W. G.; Kassel, W. S.; Rakowski DuBois, M.; DuBois, D. L.; Bullock, R. M. *Inorg. Chem.* **2011**, *50*, 10908–10918.
(24) Kilgore, U. J.; Roberts, J. A. S.; Pool, D. H.; Appel, A. M.; Stewart, M. P.; Rakowski DuBois, M.; Dougherty, W. G.; Kassel, W. S.; Bullock, R. M.; DuBois, D. L. *J. Am. Chem. Soc.* **2011**, *133*, 5861–5872.
(25) Helm, M. L.; Stewart, M. P.; Bullock, R. M.; Rakowski DuBois, M.; DuBois, D. L. *Science* **2011**, *333*, 863–866.
(26) Wilson, A. D.; Shoemaker, R. K.; Miedaner, A.; Muckerman, J. T.; DuBois, D. L.; Rakowski DuBois, M. *Proc. Natl. Acad. Sci. U. S. A.* **2007**, *104*, 6951–6956.
(27) Small, Y. A.; DuBois, D. L.; Fujita, E.; Muckerman, J. T. *Energy Environ. Sci.* **2011**, *4*, 3008–3020.
(28) Rakowski DuBois, M.; DuBois, D. L. *C. R. Chim.* **2008**, *11*, 805–817.
(29) Kaur-Ghumaan, S.; Schwartz, L.; Lomoth, R.; Stein, M.; Ott, S. *Angew. Chem., Int. Ed.* **2010**, *49*, 8033–8036.
(30) Gloaguen, F. d. r.; Lawrence, J. D.; Rauchfuss, T. B. *J. Am. Chem. Soc.* **2001**, *123*, 9476–9477.
(31) Vrubel, H.; Merki, D.; Hu, X. *Energy Environ. Sci.* **2012**, *5*, 6136–6144.
(32) Karunadasa, H. I.; Montalvo, E.; Sun, Y.; Majda, M.; Long, J. R.; Chang, C. J. *Science* **2012**, *335*, 698–702.
(33) Merki, D.; Hu, X. *Energy Environ. Sci.* **2011**, *4*, 3878–3888.
(34) Karunadasa, H. I.; Chang, C. J.; Long, J. R. *Nature* **2010**, *464*, 1329–1333.
(35) Dempsey, J. L.; Winkler, J. R.; Gray, H. B. *J. Am. Chem. Soc.* **2010**, *132*, 16774–16776.
(36) Marinescu, S. C.; Winkler, J. R.; Gray, H. B. *Proc. Natl. Acad. Sci. U. S. A.* **2012**, *109*, 15127–15131.
(37) Dempsey, J. L.; Winkler, J. R.; Gray, H. B. *J. Am. Chem. Soc.* **2010**, *132*, 1060–1065.
(38) Zhang, P.; Jacques, P.-A.; Chavarot-Kerlidou, M.; Wang, M.; Sun, L.; Fontecave, M.; Artero, V. *Inorg. Chem.* **2012**, *51*, 2115–2120.
(39) Valdez, C. N.; Dempsey, J. L.; Brunschwig, B. S.; Winkler, J. R.; Gray, H. B. *Proc. Natl. Acad. Sci. U. S. A.* **2012**, *109*, 15589–15593.
(40) Baffert, C.; Artero, V.; Fontecave, M. *Inorg. Chem.* **2007**, *46*, 1817–1824.
(41) Probst, B.; Kolano, C.; Hamm, P.; Alberto, R. *Inorg. Chem.* **2009**, *48*, 1836–1843.
(42) Solis, B. H.; Hammes-Schiffer, S. *Inorg. Chem.* **2014**, *53*, 6427–6443.
(43) Solis, B. H.; Hammes-Schiffer, S. *Inorg. Chem.* **2011**, *50*, 11252–11262.
(44) Muckerman, J. T.; Fujita, E. *Chem. Commun.* **2011**, *47*, 12456–12458.
(45) Sun, Y.; Sun, J.; Long, J. R.; Yang, P.; Chang, C. J. *Chem. Sci.* **2013**, *4*, 118–124.

DOI: 10.1021/ic5031137
Inorg. Chem. 2015, 54, 4310–4321

(46) Singh, W. M.; Mirmohades, M.; Jane, R. T.; White, T. A.; Hammarstrom, L.; Thapper, A.; Lomoth, R.; Ott, S. *Chem. Commun.* **2013**, *49*, 8638−8640.
(47) Shan, B.; Baine, T.; Ma, X. A. N.; Zhao, X.; Schmehl, R. H. *Inorg. Chem.* **2013**, *52*, 4853−4859.
(48) Rodenberg, A.; Orazietti, M.; Probst, B.; Bachmann, C.; Alberto, R.; Baldridge, K. K.; Hamm, P. *Inorg. Chem.* **2015**, *54*, 646−657.
(49) Probst, B.; Guttentag, M.; Rodenberg, A.; Hamm, P.; Alberto, R. *Inorg. Chem.* **2011**, *50*, 3404−3412.
(50) Bachmann, C.; Guttentag, M.; Spingler, B.; Alberto, R. *Inorg. Chem.* **2013**, *52*, 6055−6061.
(51) Vennampalli, M.; Liang, G.; Katta, L.; Webster, C. E.; Zhao, X. *Inorg. Chem.* **2014**, *53*, 10094−10100.
(52) Varma, S.; Castillo, C. E.; Stoll, T.; Fortage, J.; Blackman, A. G.; Molton, F.; Deronzier, A.; Collomb, M.-N. *Phys. Chem. Chem. Phys.* **2013**, *15*, 17544−17552.
(53) Deponti, E.; Luisa, A.; Natali, M.; Iengo, E.; Scandola, F. *Dalton Trans.* **2014**, *43*, 16345−16353.
(54) Becke, A. D. *Phys. Rev. A* **1988**, *38*, 3098−3100.
(55) Lee, C. T.; Yang, W. T.; Parr, R. G. *Phys. Rev. B* **1988**, *37*, 785−789.
(56) Becke, A. D. *J. Chem. Phys.* **1993**, *98*, 5648−5652.
(57) Vosko, S. H.; Wilk, L.; Nusair, M. *Can. J. Phys.* **1980**, *58*, 1200−1211.
(58) Marenich, A. V.; Cramer, C. J.; Truhlar, D. G. *J. Phys. Chem. B* **2009**, *113*, 6378−6396.
(59) Hehre, W. J.; Radom, L.; Schleyer, P. v. R.; Pople, J. A. *Ab Initio Molecular Orbital Theory;* Wiley: New York, 1986.
(60) Frisch, M. J.; Trucks, G. W.; Schlegel, H. B.; Scuseria, G. E.; Robb, M. A.; Cheeseman, J. R.; Scalmani, G.; Barone, V.; Mennucci, B.; Petersson, G. A.; Nakatsuji, H.; Caricato, M.; Li, X.; Hratchian, H. P.; Izmaylov, A. F.; Bloino, J.; Zheng, G.; Sonnenberg, J. L.; Hada, M.; Ehara, M.; Toyota, K.; Fukuda, R.; Hasegawa, J.; Ishida, M.; Nakajima, T.; Honda, Y.; Kitao, O.; Nakai, H.; Vreven, T.; Montgomery, J. A., Jr; Peralta, J. E.; Ogliaro, F. o.; Bearpark, M. J.; Heyd, J.; Brothers, E. N.; Kudin, K. N.; Staroverov, V. N.; Kobayashi, R.; Normand, J.; Raghavachari, K.; Rendell, A. P.; Burant, J. C.; Iyengar, S. S.; Tomasi, J.; Cossi, M.; Rega, N.; Millam, N. J.; Klene, M.; Knox, J. E.; Cross, J. B.; Bakken, V.; Adamo, C.; Jaramillo, J.; Gomperts, R.; Stratmann, R. E.; Yazyev, O.; Austin, A. J.; Cammi, R.; Pomelli, C.; Ochterski, J. W.; Martin, R. L.; Morokuma, K.; Zakrzewski, V. G.; Voth, G. A.; Salvador, P.; Dannenberg, J. J.; Dapprich, S.; Daniels, A. D.; Farkas, Ö.; Foresman, J. B.; Ortiz, J. V.; Cioslowski, J.; Fox, D. J.; *Gaussian 09,* Revision B.02; Gaussian, Inc.: Wallingford, CT, 2009.
(61) Tissandier, M. D.; Cowen, K. A.; Feng, W. Y.; Gundlach, E.; Cohen, M. H.; Earhart, A. D.; Coe, J. V.; Tuttle, T. R. *J. Phys. Chem. A* **1998**, *102*, 7787−7794.
(62) Camaioni, D. M.; Schwerdtfeger, C. A. *J. Phys. Chem. A* **2005**, *109*, 10795−10797.
(63) Kelly, C. P.; Cramer, C. J.; Truhlar, D. G. *J. Phys. Chem. B* **2006**, *110*, 16066−16081.
(64) Bryantsev, V. S.; Diallo, M. S.; Goddard Iii, W. A. *J. Phys. Chem. B* **2008**, *112*, 9709−9719.
(65) Bartmess, J. E. *J. Phys. Chem.* **1994**, *98*, 6420−6424.
(66) Polyansky, D. E.; Cabelli, D.; Muckerman, J. T.; Fukushima, T.; Tanaka, K.; Fujita, E. *Inorg. Chem.* **2008**, *47*, 3958−3968.
(67) Lymar, S. V.; Schwarz, H. A. *J. Phys. Chem. A* **2012**, *116*, 1383−1389 and references therein.
(68) Dadci, L.; Elias, H.; Frey, U.; Hornig, A.; Koelle, U.; Merbach, A. E.; Paulus, H.; Schneider, J. S. *Inorg. Chem.* **1995**, *34*, 306−315.
(69) Creutz, C.; Schwarz, H. A.; Wishart, J. F.; Fujita, E.; Sutin, N. *J. Am. Chem. Soc.* **1991**, *113*, 3361−3371.
(70) Creutz, C.; Schwarz, H. A.; Sutin, N. *J. Am. Chem. Soc.* **1984**, *106*, 3036−3037.
(71) Reeve, W.; Erikson, C. M.; Aluotto, P. F. *Can. J. Chem.* **1979**, *57*, 2747−2754.
(72) Tait, A. M.; Hoffman, M. Z.; Hayon, E. *J. Am. Chem. Soc.* **1976**, *98*, 86−93.
(73) Fujita, E.; Wishart, J. F.; van Eldik, R. *Inorg. Chem.* **2002**, *41*, 1579−1583.
(74) Bielski, B. H. J. In *Ascorbic Acid: Chemistry, Metabolism, and Uses;* American Chemical Society: Washington, DC, 1982; Vol. *200*, pp 81−100.
(75) Creutz, C. *Inorg. Chem.* **1981**, *20*, 4449−4452.
(76) Tamaki, Y.; Koike, K.; Morimoto, T.; Ishitani, O. *J. Catal.* **2013**, *304*, 22−28.
(77) Fourmond, V.; Jacques, P.-A.; Fontecave, M.; Artero, V. *Inorg. Chem.* **2010**, *49*, 10338−10347.
(78) Polyansky, D. E.; Muckerman, J. T.; Rochford, J.; Zong, R. F.; Thummel, R. P.; Fujita, E. *J. Am. Chem. Soc.* **2011**, *133*, 14649−14665.
(79) Guttentag, M.; Rodenberg, A.; Bachmann, C.; Senn, A.; Hamm, P.; Alberto, R. *Dalton Trans.* **2013**, *42*, 334−337.
(80) King, A. E.; Surendranath, Y.; Piro, N. A.; Bigi, J. P.; Long, J. R.; Chang, C. J. *Chem. Sci.* **2013**, *4*, 1578−1587.
(81) Zanello, P. *Inorganic Electrochemistry: Theory, Practice and Application;* The Royal Society of Chemistry: Cambridge, U.K., 2003.
(82) Olsson, M. H. M.; Ryde, U.; Roos, B. O. *Protein Sci.* **1998**, *7*, 2659−2668.
(83) Sutin, N. In *Progress in Inorganic Chemistry: An Appreciation of Henry Taube;* Lippard, S. J., Ed.; John Wiley & Sons, Inc: Hoboken, NJ, 2007; Vol. *30*, p 441−498.

DOI: 10.1021/ic5031137
Inorg. Chem. 2015, 54, 4310−4321